ATP Occlusion by P-Glycoprotein as a Surrogate Measure for Drug Coupling[†]

Gregory Tombline,*[,‡,§] Jason J. Holt,[‡] Michael K. Gannon,[‡] David J. Donnelly,[‡] Bryan Wetzel,[‡] Geri A. Sawada,[△] Thomas J. Raub,[△] and Michael R. Detty*[,‡]

Department of Chemistry, University at Buffalo, The State University of New York, Buffalo, New York 14260-3000, Department of Microbiology and Immunology, University of Rochester Medical Center, 601 Elmwood Avenue, P.O. Box 607, Rochester, New York 14642, and Drug Disposition, Eli Lilly and Company, Indianapolis, Indiana 46285

Received October 23, 2007; Revised Manuscript Received January 17, 2008

ABSTRACT: The multidrug efflux pump P-glycoprotein (Pgp) couples drug transport to ATP hydrolysis. Previously, using a synthetic library of tetramethylrosamine (**TMR**) analogues, we observed significant variation in ATPase stimulation (V_m^D). Concentrations required for half-maximal ATPase stimulation (K_m^D) correlated with ATP hydrolysis transition-state stabilization and ATP occlusion (EC_{50}^D) at a single site. Herein, we characterize several **TMR** analogues that elicit modest turnover ($k_{cat} \leq 1$–$2\ s^{-1}$) compared to verapamil (VER) ($k_{cat} \sim 10\ s^{-1}$). Apparent ATPase activities manifest as nearly equivalent to basal values. In some cases, K_m^D parameters for drug stimulation of ATPase could not be accurately determined, yet these same **TMR** analogues promoted ATP occlusion at relatively low concentrations (~0.4–40 μM). Moreover, the **TMR** analogues competitively inhibited VER-dependent ATPase activity at concentrations similar to those required for ATP occlusion. Finally, the **TMR** analogues facilitated uptake of calcein-AM into CR1R12 and MDCK-MDR1 cells and are actively transported by Pgp in monolayers of MDCK-MDR1 cells at similarly low concentrations (~1–20 μM). ADP·V_i release kinetics were identical in the presence of the **TMR** derivatives, VER, or in the absence of drug, suggesting that slow turnover is not likely due to slow release of the ATP hydrolysis products ADP and P_i. These data support the partition model in which drug site occupancy converts residual basal ATPase activity to a drug-dependent mechanism even in cases where stimulation appears to be exactly compensatory to basal values. It is noteworthy that when compared to previously reported **TMR** analogues, subtle modification of the **TMR** scaffold can confer large differences in ATP turnover.

P-Glycoprotein (Pgp,[1] MDR1, or ABCB1) is a plasma membrane-located efflux pump that confers multidrug resistance (MDR) against a variety of diverse chemotherapeutic drugs. Cancers that display drug resistance are refractory to treatment. Excellent reviews of Pgp biology, drug design, and current thoughts regarding mechanism are available (*1*–*9*). Although efforts to study Pgp have generated more than 10000 published papers (current Medline search), the lack of a high-resolution structure, the lack of a precise mechanism of transport, and the failure to develop potent, clinically useful inhibitors have spawned a jaded attitude for future progress by drug companies (*10*). Yet, a growing number of ATP binding cassette (ABC) transporters (of 48 total in humans) confer drug resistance in cell culture. Although their clinical relevance remains uncertain (*11, 12*), they are homologous to Pgp. Thus, Pgp studies will likely have broad relevance clinically. Similarly, understanding of other ABC transporters that serve diverse physiological functions (other than MDR) and whose clinical relevance is well-established due to hereditary disease may also be advanced (*13, 14*).

Several models derived from an early "alternating-sites model" (*15*) have been proposed in an effort to explain how Pgp couples binding and hydrolysis of ATP at the two nucleotide binding domains (NBDs) to drug export by the transmembrane domains (TMDs) (*4, 5, 16*–*18*). Several key aspects remain unclear. How is the chemical energy derived from ATP binding and hydrolysis at NBD catalytic sites coordinated with conformational changes in the TMDs to permit transport of drugs? How does Pgp transport a diversity of drugs? Drugs with diverse structures are transported at different rates, yet the process occurs through a common transition state (*19*). This begs the following question: What

[†] This research was supported in part by NIH Grant T32 CA09363 (Postdoctoral Training Grant) to G.T. and by the Department of Defense (Breast Cancer Research Program) under Award W81XWH-04-1-0708 to M.R.D. and Award W81XWH-04-1-0368 to D.J.D. and M.K.G.

* To whom correspondence should be addressed. G.T.: current address, Department of Microbiology and Immunology, University of Rochester Medical Center, 601 Elmwood Ave., P.O. Box 607, Rochester, NY 14642; telephone, (585) 275-0676; fax, (585) 473-9573; e-mail, gregory_tombline@urmc.rochester.edu. M.R.D.: telephone, (716) 645-6800, ext. 2200; fax, (716) 645-6963; e-mail, mdetty@buffalo.edu.

[‡] University at Buffalo, The State University of New York.

[§] University of Rochester Medical Center.

[△] Eli Lilly and Company.

[1] Abbreviations: Pgp, P-glycoprotein; BSA, bovine serum albumin; DMSO, dimethyl sulfoxide; EC_{50}, molar concentration that produces 50% of the maximal stimulatory response; EGTA, ethylene glycol tetraacetic acid; EM, electron microscopy; FBS, fetal bovine serum; FRET, fluorescence resonance energy transfer; H/D, hydrogen/deuterium; IC_{50}, molar concentration that produces 50% of the maximal inhibitory response; NBD, nucleotide binding domain; ONC, occluded nucleotide conformation; TMD, transmembrane domain; TMR, tetramethylrosamine; V_i, vanadate anion; VER, verapamil; NBD-Cl, 7-chloro-4-nitrobenzo-2-oxa-1,3-diazole; NEM, *N*-ethylmaleimide; DM, *N*-dodecyl β-D-maltoside; THF, tetrahydrofuran; Tris, tris(hydroxymethyl)aminomethane.

10.1021/bi7021393 CCC: $40.75
Published on Web 02/15/2008

is the pharmacophore (or catalog of molecular descriptors) that enables drug transport at a particular rate? This is a complicated question given the diversity of drugs transported by Pgp and the fact that competitive and noncompetitive interactions within the drug pocket exist (*9, 20, 21*), as well as allosteric sites that appear to reside outside the common pocket (*22, 23*). Many attempts to answer these questions using computational approaches have been made, yet there is no clear consensus for an algorithm for predicting substrates and inhibitors (*7, 24, 25*).

An interesting property of many drugs that bind to Pgp is that they initially stimulate hydrolysis (with concomitant transport) yet, at very high concentrations, become inhibitory to ATPase activity (and transport slows) (*26, 27*). Half-maximal values for ATPase stimulation and inhibition are K_m^D and K_i^D, respectively. Pgp reconstituted into inside-out vesicles establishes drug transport gradients, the value being the ratio of K_i^D/K_m^D (*19*). EPR spectroscopy studies of spin-labeled VER indicate that K_m^D reflects affinity at "ON" sites (*28*). In their "solvation exchange model", Omote and Al-Shawi (*18*) bolster the idea that ON sites are points of initial recognition located on the outside of TMD helices. Consistent with the "vacuum-cleaner" model for drug transport (*29*), molecular dynamics simulation of drug movement through a model bilayer predicts that ON sites are located at points of contact with the inner leaflet of the membrane (*18*). As noted by Seelig (*7*), H-bonding and charge interactions between Pgp and drugs will be enhanced due to the electrostatic environment of the bilayer. Seelig's group generated a pharmacophore model for Pgp−drug interactions suggesting that affinity is strongly influenced by the number of H-bonding donor/acceptor pairs and that the rate of turnover increases as the number of H-bonding groups increases until a certain threshold, beyond which the rate of turnover decreases (*7, 30*). At very high concentrations of drugs, release from OFF sites may affect turnover. Experimental evidence and modeling efforts prompted Omote and Al-Shawi to suggest that at very high drug concentrations, K_i^D reflects affinity at OFF sites located within an inner cavity or "vestibule" (*18*).

An important goal is to develop an atomic-detail model of Pgp drug transport that will integrate rate data with structural changes. Several elegant approaches, including EM (*31–34*), cross-linking (*35, 36*), H/D exchange (*37*), mAb binding to the unique epitope UIC2 (*38, 39*), fluorescence quenching (*40, 41*), and fluorescence resonance energy transfer (FRET) studies (*42*), support coordinated conformational changes during the catalytic cycle. Excellent recent reviews on this topic and their relationship to mechanism are available (*4, 5, 43*). For example, cross-linking studies indicate drugs that stimulate Pgp ATPase activity elicit conformational changes that "engage" the catalytic sites by bringing Walker A residues of NBD1 closer to LSGGQ motif Ser residues of the neighboring NBD2 and vice versa (*36*). Reciprocally, ADP·V_i trapping at catalytic sites causes a change in MTS cross-linking at TMDs, suggesting that during ATP hydrolysis, TM helices rotate perhaps altering the affinity of drug sites from high to low (*35*). We have provided evidence that drugs elicit the transition to an asymmetric occluded nucleotide conformation (ONC) and that this intermediate normally occurs transiently during the catalytic cycle (*44–46*). Support for the ONC as a genuine state was bolstered recently by Sauna et al. (*47*), who demonstrated that the relatively nonhydrolyzable ATP analogue, ATPγS, is occluded by wild-type human Pgp.

Chart 1: Structure of **TMR** and 9-(2-Thienyl-5-diethylcarboxamide)chalcogenoxanthylium Derivatives **1**

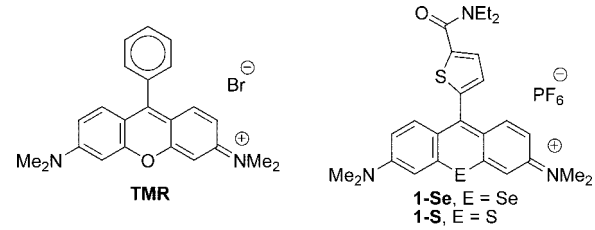

Our aim is to generate pharmacophore models of drug-binding sites that determine kinetic parameters of ATP-coupled transport and correlate the occupancy of these sites with the conformation of Pgp during the catalytic cycle. This kind of knowledge will likely reveal the trajectory of drug during the transport process and will permit a clear understanding of the physical basis for coupling. A corollary is that elucidation of the pharmacophores that determine these sites may enable the design of a tightly bound drug that slows the rate of turnover to very low levels (near zero) while competitively excluding other chemotherapeutic drugs from binding to Pgp.

In a previous manuscript, we presented a library of analogues of the rhodamine-related tetramethylrosamine (**TMR**, Chart 1) that displayed 2−3 order of magnitude differences in their ability to promote ATP turnover (*48*). For this reason, and since almost all drugs have been assayed for competitive transport with rhodamines in the NCI screen (*49, 50*), further development of **TMR** analogues to pursue questions related to ATPase (and transport) rate enhancement was initiated. Herein, we examine a smaller set of **TMR** analogues with a limited apparent ability to stimulate ATPase, yet their abilities to promote ATP occlusion, competitively inhibit verapamil-dependent ATPase activity, and be transported in cells reveal their true affinities for Pgp.

EXPERIMENTAL PROCEDURES

General. All chemicals and reagents were purchased from Sigma Chemical Co. (St. Louis, MO) unless otherwise noted. Elemental analyses were conducted by Atlantic Microlabs, Inc. (Norcross, GA). **TMR-S** and **TMR-Se** were prepared according to ref *51*. Dye **1-S** was prepared according to ref *48*. Selenoxanthylium dyes **2** and **4** were prepared according to ref *52*. Selenoxanthone **7** was prepared according to ref *53*. Chalcogenoxanthylium dyes **5** and **6** were prepared according to ref *54*.

Synthesis of 3,6-Bis(dimethylamino)-9-(4-N-morpholinophenyl)selenoxanthylium Hexafluorophosphate (3). A solution of 4-(4-bromophenyl)morpholine (1.0 g, 4.3 mmol) in 2 mL of anhydrous THF was added to a stirred mixture (0.110 g, 4.4 mmol) of ground magnesium turnings in 10 mL of anhydrous THF. The resulting mixture was heated at reflux for 2 h, cooled to ambient temperature, and then added dropwise via cannula to a stirred solution of 3,6-bis(dimethylamino)-9*H*-selenoxanthen-9-one (**7**, 0.150 g, 0.43 mmol) in anhydrous THF (3.0 mL). The resulting mixture was

Table 1: Summary of Data for **TMR-Se** and Compounds **2–6**[a]

compd	ATPase[b] V_M (nmol min^{-1} μg^{-1}) (MDR3 CL)	ATPase K_m^D (μM) (MDR3 CL)	ATP occlusion EC_{50}^D (μM) (MDR3 A/A)	ATPase inhibition IC_{50}[c] (μM) (MDR3 CL)	ATPase inhibition K_i (μM) (MDR3 CL)	CAM uptake EC_{50}^{CAM} (μM) (CHO MDR1)
TMR-Se	0.93 ± 0.20	74 ± 19	14 ± 7	–	–	–
2	1.16 ± 0.16	288 ± 115	43 ± 37	21 ± 1	8 ± 1	–
3	0.62 ± 0.13[d]	ND[d]	20 ± 11	23 ± 8	10 ± 2	7 ± 5
4	0.37 ± 0.07[d]	ND[d]	0.4 ± 0.2	30 ± 7	10 ± 2	16 ± 1 2
5	1.10 ± 0.20	100 ± 58	9 ± 4	0.28 ± 0.07[e]	2.0 ± 0.4	0.8 ± 0.3
6	0.83 ± 0.10	78 ± 34	7 ± 5	15 ± 4	7 ± 2	1.0 ± 0.5

[a] Data include maximal ATPase activity (V_M), as well as the concentration of drug required to confer half-maximal ATPase activity (K_m^D) by mouse MDR3 Cys-less Pgp. V_M and K_m^D parameters were obtained by fitting the data to a partition function as detailed in Experimental Procedures. For comparison, basal and VER-stimulated ATPase activities were 0.35 ± 0.05 and 3.9 ± 0.2 nmol min^{-1} μg^{-1}, respectively. Also shown are values for the concentration of analogue required for half-maximal ATP occlusion (EC_{50}^D) by E552A/E1197A mouse MDR3 Pgp, and values for inhibition of VER-dependent ATPase activity (IC_{50} and K_i). The concentration of the **TMR** analogue required for half-maximal uptake of CAM (EC_{50}^{CAM}) into the Chinese hamster ovary CR1R12 cell line is indicated. Details for methods are provided in Experimental Procedures, and figures show original data. [b] ATPase values were from the spectrophotometric coupled microplate assay where NADH oxidation was assessed. Original data for these values are shown in the figures. [c] Inhibition in the presence of a fixed concentration (200 μM) of VER. [d] V_M values for compounds **3** and **4** were the maximum activity displayed at a single point, and K_m^D values are not determined since fitting the entire data set to the partition model failed to yield reliable values. [e] This value is the midpoint of the first exponential phase of inhibition after data were fit to two exponentials (see Figure 3a).

heated at reflux for 0.5 h, cooled to ambient temperature, and poured into acetic acid (3.0 mL). Hexafluorophosphoric acid (60% weight solution in water) was added dropwise until a color change was observed. Water (50 mL) was added, and the solution was cooled to −10 °C. The precipitate was collected by filtration, washed with water (10 mL) and diethyl ether (10 mL), and then recrystallized from acetonitrile and a small amount of ether to give 0.085 g (53%) of **3** as a dark green solid: mp 270–271 °C; ^{1}H NMR (400 MHz, CD_2Cl_2) δ 7.61 (d, 2 H, J = 9.5 Hz), 7.58 (d, 2 H, J = 2.5 Hz), 7.22 (d, 2 H, J = 8.4 Hz), 7.12 (d, 2 H, J = 8.4 Hz), 6.89 (d × d, 2 H, J = 2.5, 9.5 Hz), 3.93 (t, 4 H, J = 4.4, 5.1 Hz), 3.34 (t, 4 H, J = 4.4, 5.1 Hz), 3.30 (s, 12 H); ^{13}C NMR (126 MHz, CD_2Cl_2) δ 155.4, 142.4, 132.5, 131.2, 128.5, 127.4, 126.0, 119.0, 114.9, 114.2, 104.1, 65.0, 46.3, 38.9; $\lambda_{max}(CH_3OH)$ = 581 nm ($\epsilon = 5.9 \times 10^4$ M^{-1} cm^{-1}); HRMS (ESI) m/z 492.15546 (calcd for $C_{25}H_{29}ON_3{}^{80}Se$, 492.1549). Anal. Calcd for $C_{25}H_{29}ON_3Se \cdot PF_6$: C, 50.95; H, 4.75; N, 6.60. Found: C, 50.56; H, 4.66; N, 6.43.

Expression, Purification, Quantitation, and Activation of Pgp. Strains of yeast *Pichia pastoris* expressing mouse mdr3 wild-type, E552A/E1197A, and Cys-less Pgp were grown in a fermentor culture and purified as described previously (*44, 55, 56*). The Pgp concentration was determined by quantitation after SDS gel electrophoresis on 10% gels and Coomassie Blue staining. Several dilutions of unknown Pgp were resolved alongside a similar series of a reference preparation whose concentration had previously been accurately determined by amino acid analysis. Protein bands were quantified with Scion Image (Scion Corp.). Pgp was stored in aliquots at −70 °C with excellent retention of activity. Just prior to each experiment, Pgp was activated by incubation with a 2:1 (w/w) equivalent of *Escherichia coli* lipids (Avanti Polar Lipids; acetone/ether-precipitated) for 20 min at room temperature followed by sonication for 30 s at 4 °C in a bath sonicator. For wild-type and E552A/E1197A proteins, 5 mM DTT was included during the 20 min incubation to reduce the inhibitory disulfide between P-loop cysteines.

ATPase Assays. ATP hydrolysis determined by the spectrophotometric coupled assay was performed in microplate format in 96-well plates as previously described (*48*). Each reaction mixture contained 4–5 μg of lipid-activated Cys-less mouse mdr3 Pgp with the indicated concentration of drug or **TMR** analogue added in a volume of 1 μL from concentrated DMSO stock solutions. Cys-less protein was routinely used for ATPase measurements for consistency and to avoid DTT, which is necessary for activation of wild-type Pgp but was found to reduce some of the compounds. DMSO was at a final concentration of 2% in all reaction mixtures. Each 50 μL reaction mixture contained 40 mM Tris-HCl (pH 7.4), 0.1 mM EGTA, 10 mM NaATP, 12 mM $MgSO_4$, 3 mM PEP, 1.5 mM NADH, and pyruvate kinase and lactate dehydrogenase (each at a final concentration of 0.1 mg/mL). Reaction mixtures were kept on ice and in the dark until they were placed in the plate reader. Kinetics of NADH oxidation was followed at 37 °C by a decrease in absorption at 340 nm, and this was converted into a specific activity for moles of ATP hydrolyzed. Control reactions that included DMSO alone or 150 μM VER were performed in parallel for comparison. Assays were performed in a Spectramax Gemini plate reader and analyzed with SOFTmaxPro. ATPase parameters were determined by fitting activities for drug titrations to the modified Michaelis–Menten equation that incorporates an initial basal activity which disappears as drug-binding sites are occupied [partition equation (*19*)] using SigmaPlot 2000 as previously described (*48*). Studies of the inhibition of VER-stimulated ATPase (for IC_{50} and K_i values) activity were essentially identical except that each reaction mixture contained 2 μg of lipid-activated Pgp. IC_{50} values were determined in the presence of 200 μM VER. For K_i values, the indicated concentration of VER was present. Just as the modified Michaelis–Menten equation was used to fit activation data, K_i values were determined by fitting the data to a modified partition equation for competitive inhibition (eq 1; see ref *57*) using SigmaPlot2000.

$$v = V_m{}^B + \{(V_m{}^D - V_m{}^B)d/[d + K_m{}^D(1 + c/K_i)]\} \quad (1)$$

This equation incorporates a basal ATPase rate (V_m^B) that is subtracted from the maximal ATPase activity in the presence of drug (V_m^D). In this case, v is the ATPase activity at a particular concentration of VER (d) and, if present, a particular concentration of the inhibitor **TMR** analogue (c). K_m^D signifies the concentration of VER required for half-maximal activity, and V_m^D signifies the maximal activity. K_i is the competitive inhibition constant for the **TMR** analogue

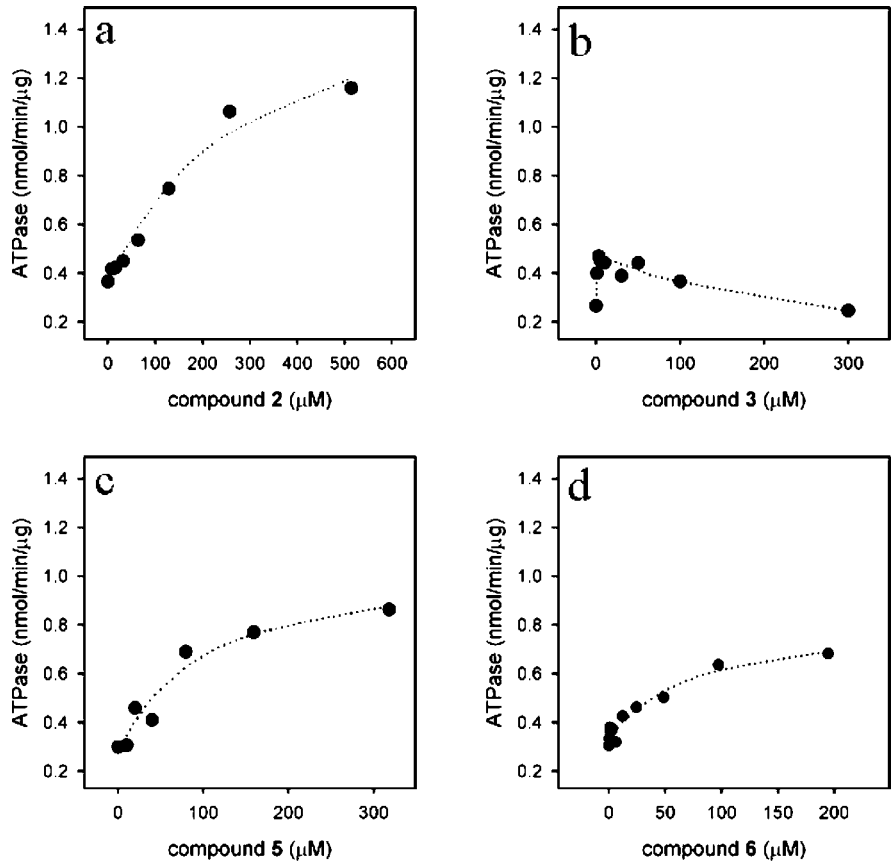

FIGURE 1: Effect of compounds **2**, **3**, **5**, and **6** on Pgp ATPase using the spectrophotometric coupled assay. The effect of compounds **2**, **3**, **5**, and **6** on Pgp activity was determined as described in Experimental Procedures. Data represent the mean of three separate experiments. Data sets showed excellent agreement with a standard deviation of less than 10% at each point.

being measured. For clarity, K_i values presented in Table 1 are distinct from the K_i^D term used previously to describe the inhibition phase of drugs that display biphasic effects on Pgp ATPase. ATPase activity was also measured by the release of [^{32}P]P_i from [γ-^{32}P]ATP using the charcoal (Norit) adsorption assay as previously described (*44, 58*). Briefly, each 50 μL reaction mixture contained 40 mM Tris-HCl (pH 7.4), 0.1 mM EGTA, 2 mM [α-^{32}P]ATP (~0.02 Ci/mmol), 4 mM $MgSO_4$, and 0.4 μg of activated Pgp as well as the indicated concentration of **TMR** analogue (or DMSO alone). The final level of DMSO was 2% in all reaction mixtures. Immediately prior to each set of assays, a cocktail containing all components except drug was prepared and kept on ice. Reactions were initiated by adding 49 μL of cocktail to 1 μL of each drug (or DMSO), and samples were incubated at 37 °C for either 10 min (VER) or 1 h (**TMR** analogues). Next, samples were placed on ice, and 400 μL of an ice-cold suspension consisting of 10% charcoal (acid-washed) and 10 mM EDTA was added. Tubes were vortexed and kept at 4 °C overnight. After centrifugation to pellet the charcoal, two 100 μL aliquots of the supernatant were removed, and the amount of [^{32}P]P_i was determined by Cerenkov counting.

ADP·V_i Trapping and Release. Drug stimulation of ADP·V_i trapping after hydrolysis (and release of phosphate) was performed as described previously (*58*) using lipid-activated mouse mdr3 wild-type Pgp (87% identical to human Pgp). This method relies on the measurement of the amount of [α-^{32}P]ADP·V_i complex retained by Pgp after it passes through a centrifuge column (tuberculin) containing

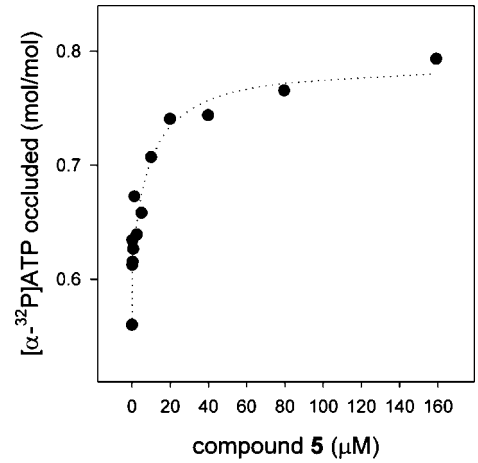

FIGURE 2: Promotion of ATP occlusion by compound **5**. The effect of compound **5** on ATP occlusion by A/A mutant Pgp was determined as described in Experimental Procedures. Data represent the mean of two separate experiments using two different preparations of A/A Pgp. Data sets showed excellent agreement with a standard deviation of less than 10% at each point.

Sephadex G-50. Drug enhancement is detected as an increase in the fraction of Pgp·ADP·V_i inhibited complex. Briefly, 10 μg of lipid- and DTT-activated wild-type Pgp was incubated in a volume of 50 μL with 40 mM Tris-HCl (pH 7.4), 0.1 mM EGTA, 200 μM [α-^{32}P]ATP, 2.2 mM $MgSO_4$, 200 μM V_i, and the indicated concentration of drug added from concentrated DMSO stocks. In all cases, the final concentration of DMSO was 2%. Samples were incubated for 10 min at 37 °C and then placed on ice for 2 min. All

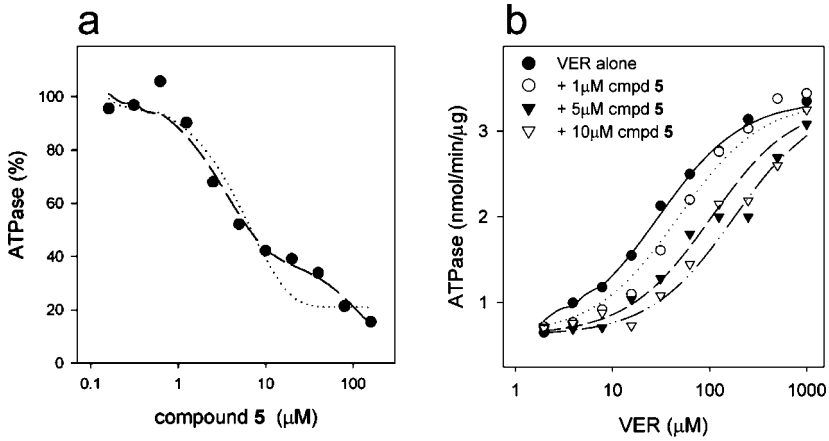

FIGURE 3: Inhibition of VER-dependent ATPase by compound **5**. (a) Inhibition of VER (200 μM)-dependent ATPase by compound **5** was assessed as described in Experimental Procedures. The dotted line is the nonlinear least-squares regression fit of the data to a single-exponential parameter which gave an IC_{50} of 3.8 $\pm$ 0.9 μM ($R^2 = 0.95$). The dashed line is the nonlinear least-squares regression fit of the data using two exponential parameters where the midpoints of each slope were 0.28 $\pm$ 0.07 and 41.8 $\pm$ 6 μM ($R^2 = 0.98$). Data represent the average of three separate experiments which showed excellent agreement (a standard deviation of less than 10% for all points). Maximal ATPase activity (100%) corresponds to the VER-dependent V_m^D value (3.9 $\pm$ 0.2 nmol min^{-1} μg^{-1}). (b) Classic competitive analysis for inhibition of VER (200 μM)-dependent ATPase by analogue **5** was conducted as described in Experimental Procedures. The lines represent the nonlinear least-squares regression fits of the data to eq 1 (see the text) and give a K_i^D of 2.0 $\pm$ 0.4 μM (see also Table 1). Data represent the average of two separate experiments which showed excellent agreement (a standard deviation of $\sim$10% for all points).

manipulations were performed in the dark. Next, 50 μL of ice-cold TE buffer [40 mM Tris-HCl (pH 7.4) and 0.1 mM EGTA] was added, and the samples were passed through centrifuge columns. Retained [α-^{32}P]ADP$\cdot V_i$ complex was quantitated by Cerenkov counting. Release of the Pgp-[α-^{32}P]ADP$\cdot V_i$ complex was assessed as previously described (*58*) except that all manipulations were performed in the dark. Briefly, 120 μg of lipid- and DTT-activated wild-type Pgp was incubated in a volume of 400 μL with 40 mM Tris-HCl (pH 7.4), 0.1 mM EGTA, 200 μM [α-^{32}P]ATP, 2.2 mM $MgSO_4$, 200 μM V_i, and 200 μM drug added from concentrated DMSO stocks for 30 min at 37 °C. After being placed on ice for 10 min, samples were divided into four 100 μL portions and passed through centrifuge columns to remove free [α-^{32}P]ADP. Eluted fractions were pooled, and 1 mL of ice-cold TE buffer with 200 μM drug was added to ensure that release of the [α-^{32}P]ADP$\cdot V_i$ complex was assayed in the presence of drug. Next, samples were divided into 12 $\times$ 100 μL aliquots and incubated at 37 °C to allow for release of the [α-^{32}P]ADP$\cdot V_i$ complex. At the indicated time, samples were placed on ice for 1 min and then passed through centrifuge columns. The [α-^{32}P]ADP$\cdot V_i$ complex was quantitated by Cerenkov counting. Release kinetics was determined by nonlinear regression fitting of the data to a single-exponential decay process using SigmaPlot.

ATP Occlusion Assay. Drug stimulation of ATP occlusion by E552A/E1197A (A/A) double "catalytic carboxylate" mutant Pgp was performed as described previously (*48*). Similar to the [α-^{32}P]ADP$\cdot V_i$ trapping studies mentioned above, this method relies on the measurement of the amount of [α-^{32}P]ATP retained by E552A/E1197A Pgp after it passes through a centrifuge column containing Sephadex G-50. Assays were identical to those described above, except that V_i was omitted and 10 μg of E552A/E1197A Pgp replaced wild-type Pgp.

*Enhancement of Uptake of Calcein-AM into CR1R12 Cells by **TMR** Analogues.* CR1R12 cells were maintained in α-MEM medium supplemented with 10% fetal bovine serum (FBS) and penicillin/streptomycin and grown at 37 °C with 5% CO_2 as previously described (*54*). Uptake of calcein-AM (CAM) was performed as described previously (*59*) except that uptake was followed kinetically for up to 2.5 h. One day prior to uptake experiments, $\sim$5–10000 cells (in a volume of 200 μL) were seeded per well on 96-well sterile tissue culture plates (Corning). After 24 h, medium was replaced and incubation continued for an additional 2 h. Next, medium was removed, and 100 μL of 0.9% NaCl containing 1 μM CAM (Invitrogen/Molecular Probes) and either DMSO or **TMR** analogue at the indicated concentration were added. The final DMSO concentration was 0.2% in all cases, and this did not affect the ability of CR1R12 cells to exclude CAM. Kinetics (every 3 min for 3 h) of CAM uptake were determined by measuring the level of conversion to the fluorescent calcein. Measurements were performed directly in the microplate with λ_{ex} and λ_{em} set to 485 and 530 nm, respectively, using a SpectraMax Gemini fluorescence plate reader. EC_{50}^D values represent relative half-maximal values for enhancement of CAM uptake obtained by fitting the raw fluorescence data to a single-exponential increase (simple hyperbolic curve) by nonlinear least-squares regression using SigmaPlot2000.

*Enhancement of Uptake of Calcein-AM into MDCK-MDR1 Cells by **TMR** Analogues.* MDCK cells transfected with wild-type MDR1 (ABCB1) were obtained at passage number 12 from P. Borst at The Netherlands Cancer Institute (Amsterdam, The Netherlands). Cell growth was maintained in Dulbecco's modified Eagle's medium (Gibco) supplemented with 10% fetal bovine serum (FBS), 100 units/mL penicillin, and 100 μg/mL streptomycin in 75 cm^2 flasks. Cultures were passaged by trypsinization 1:10 twice a week and used at passage number 16-42. Cells were seeded at a density of 40000 cells/well in 96-well flat bottom plates (Falcon) using a medium volume of 200 μL, which was replaced on day 3 prior to their use on day 4.

Cells were washed once with Dulbecco's phosphate-buffered saline containing 10 mM Hepes buffer at pH 7.4 (DPBSH) (Gibco) and incubated with solutions of the **TMR** analogue in DPBSH at 37 °C under room atmosphere. EC_{50}

Chart 2: Structure of Selenoxanthone **7**

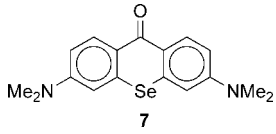

7

values were calculated from 1:1 serial dilution series. After 30 min, the test compound was replaced to include 0.5 μg/mL CAM and incubated for an additional 20 min. Calcein fluorescence was read on a Cytofluor series 4000 multiwell plate reader (PerSeptive Biosystems) with λ_{ex} and λ_{em} set to 485 and 530 nm, respectively. Negative (0.25% DMSO in DPBSH) and positive (2.5 μM LSN335984, a specific Pgp inhibitor) controls were included in each plate. EC_{50} values were calculated from the serial dilution curves using GraphPad PRISM, version 4.03. Briefly, the compound concentration was plotted as log micromolar concentration versus relative fluorescence units (rfu), and a sigmoidal dose–response (variable slope) analysis with no weighting or restrictions was applied.

Studies of Transport of Pgp across MDCK-MDR1 Monolayers. MDCK-MDR1 cells that were seeded at a density of 50000 cells/cm^2 onto 12-well (1.13 cm^2 surface area) Transwell polycarbonate filters (Costar) were fed on days 3 and 5 and used on day 6. The upper and lower chamber volumes were 0.5 and 1.0 mL, respectively. Cells were rinsed for 10 min in DPBSH at 37 °C with mixing on a nutator (Clay Adams). Cells were preincubated with 4.3 mg/mL bovine serum albumin (BSA) in DPBSH with or without 2.5 μM LSN335984. After 30 min, 5 μM test compound in BSA/DPBSH with or without inhibitor was added to the donor chamber (0.5 mL upper or apical, 1.0 mL lower or basolateral). Initial donor samples were taken at time zero. For apical-to-basolateral (A−B) flux, D_0 was taken from the mixing tube before addition to the cell monolayer. For basolateral-to-apical (B−A) flux, this sample was taken from the 12-well plate 10 min after transfer, but before cell wells were added. Samples were taken from both the donor and receiver chambers following a 1 h incubation at 37 °C with constant mixing by nutation. Cell monolayers were rinsed briefly two times using cold DPBS and extracted with 500 μL of methanol for 3 min. All sample volumes were 200 μL, and samples were transferred directly to a black-wall, flat bottom 96-well plate (Costar). The plate was centrifuged for 5 min at 1500 rpm to reduce bubbles and then analyzed using a Spectromax M2 fluorescent plate reader (Molecular Devices) at individually optimized excitation and emission wavelengths. For **TMR** and **TMR-S**, λ_{ex} and λ_{em} were set to 554 and 590 nm, respectively. For **1-S** (Chart 1), **5** (Chart 3), and **6** (Chart 3), λ_{ex} and λ_{em} were set to 584 and 612 nm, respectively.

RESULTS

*Synthesis of Novel **TMR** Analogues.* Recently, we examined a small library of chalcogenoxanthylium analogues of **TMR** for their ability to stimulate Pgp ATPase activity (*48*). Importantly, using occlusion of ATP by A/A Pgp, a strong correlation between K_m^D for stimulation of ATPase activity and the concentration of drug (EC_{50}^D) required to promote ATP occlusion at a single catalytic site was found for the parental analogue **TMR-S** ($K_m^D \sim EC_{50}^D \sim 100$ μM), as

Chart 3: Structures of Chalcogenoxanthylium Analogues of **TMR** Used in This Study

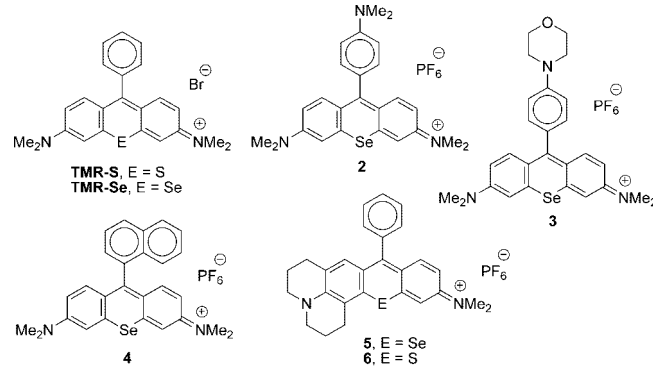

well as derivative **1-Se** with a 2-thienyl-5-(diethylcarboxamide) group at the 9-position of the xanthylium core [Chart 1, compound **22** in a previous study (*48*); $K_m^D \sim EC_{50}^D \sim$ 3–6 μM], and verapamil (VER; $K_m^D \sim EC_{50}^D \sim 10$ μM). These data suggested that binding parameters that determine K_m^D for ATPase stimulation may represent the transition to the occluded nucleotide conformation. In addition, slight modification of **TMR** analogues greatly influenced K_m^D as well as turnover, suggesting that the **TMR** scaffold may provide a useful starting point for a pharmacophore.

To test the generality of these conclusions, herein we examine several analogues of **TMR** that either displayed a relatively high K_m^D or showed relatively weak stimulation of ATPase in the first study (*48*) as well as newer derivatives that also fail to elicit robust ATPase activity. The structures of the **TMR** analogues used in this study are shown in Chart 3. Our earlier work demonstrated that subtle changes in substituents at the 9-position of the **TMR** scaffold produced large differential effects in stimulatory capacity. The results also indicated that 4-dialkylaminophenyl and large hydrophobic groups such as the 1-naphthyl substituent in the 9-position elicited little stimulation of ATPase activity (*48*). Herein, in addition to the 9-(4-dimethylaminophenyl)selenoxanthylium derivative **2**, we have also examined the 9-(4-*N*-morpholinophenyl)selenoxanthylium derivative **3** as a modification of the alkyl groups on the dimethylamino substituent. The selenoxanthylium analogue **TMR-Se** has a 9-phenyl substituent as a hydrophobic group. We also examined the 9-(1-naphthyl)selenoxanthylium derivative **4** as an analogue of **TMR-Se** with a larger hydrophobic group at the 9-position. We were able to increase the hydrophobicity of **TMR-S** and **TMR-Se** through propano bridges that tie the amino alkyl substituents to the xanthylium core with pentacyclic selenoxanthylium derivative **5** and pentacyclic thioxanthylium derivative **6**.

*Effect of **TMR** Analogues on Pgp ATPase Activity.* Table 1 summarizes the effect of structural modifications of the **TMR** analogues on Pgp ATPase activity, occlusion of ATP by E552A/E1197A mdr3 Pgp, and apparent inhibitory effects, which will be presented below. ATPase values listed in Table 1 were determined using the spectrophotometric coupled assay, and profiles for derivatives **2**, **3**, **5**, and **6** are found in Figure 1. Typical profiles for ATPase stimulation by VER, **TMR-Se**, and derivative **4** may be found in a previous study (*48*). Derivative **2** displayed the most robust stimulation among the group as the ATPase value was approximately 4 times the basal value. Derivatives **3** and **4**

displayed the weakest ATPase stimulation among the group with ATPase activities that manifest at near-basal levels. In these cases, K_m^D values could not be accurately ascertained and a partition model fit of the data is not likely to be reliable. Derivatives **5** and **6** displayed ATPase activities that manifest as approximately twice the basal value. In general, all of the derivatives displayed significantly less activity compared to VER or other **TMR** analogues that were characterized previously (*48*) whose activities are relatively robust and manifest as values approximately 10-fold higher than basal levels. This ratio was consistent in this study since the basal ATPase activity was ~0.35 nmol min^{-1} μg^{-1}, and in the presence of 200 μM VER, ATPase activity was routinely ~3.9 nmol min^{-1} μg^{-1}. Several wells containing basal and VER controls were included in each microplate assay to ensure relative values. Since the spectrophotometric coupled assay is relatively insensitive to turnover rates that are less than 1–2 s^{-1}, we also employed a more sensitive charcoal adsorption assay (Norit) for **TMR** analogues whose turnover values fell below this threshold and for which K_m^D could not be accurately determined by the coupled assay (*44, 58*). An additional motivation was to employ a separate assay to examine the derivatives whereby phosphate production was directly assessed. Basal and VER-induced (200 μM) ATPase activities were ~0.15 and ~0.9 nmol min^{-1} μg^{-1}, respectively. Derivatives **3**−**6** (which displayed near-basal ATPase activity in the spectrophotometric assay) all failed to display ATPase activities that were significantly greater than the basal level (data not shown). These data further suggest that these **TMR** derivatives display ATPase activities which are nearly compensatory to basal values.

*Effect of **TMR** Analogues on Pgp ATP Occlusion.* Using a "catalytic carboxylate" mutant A/A (mdr3 E552A/E1197A) Pgp defective in hydrolysis, we provided evidence in earlier studies that the occluded nucleotide conformation (ONC) is (1) likely to occur transiently during the normal catalytic cycle and (2) a key conformation involved in the coupling of drug binding at TMDs with NBD catalytic sites (*44–46*). The likely scenario is that drugs elicit engagement of a NBD dimer similar to NBD dimers seen in crystal structures of bacterial ABC proteins (*60–63*). One distinction that we emphasized previously is that the engaged NBD dimer (ONC) is asymmetric in intact Pgp due to interdomain communication between the TMDs and NBDs (*46*). Moreover, this scenario contrasts cases of isolated NBDs in which such communication is absent. A molecular dynamics simulation of ATP binding by the bacterial vitamin B_{12} uptake transporter (BtuCD) (*64*) suggests that all intact ABC transporters may progress to an asymmetric state during catalysis.

Interestingly, many **TMR** analogues that appear ineffective at promoting robust ATP turnover are, in fact, relatively proficient at promoting ATP occlusion. Among the first analogues examined for stimulation of ATP occlusion was **TMR-Se**. While the K_m^D (74 ± 19 μM) for **TMR-Se** was not dramatically different from the K_m^D for **TMR-S**, turnover was significantly slower [0.93 ± 0.20 nmol min^{-1} μg^{-1}, Table 1, and previous data (*48*)]. Unlike results with **TMR-S** where $K_m^D \sim EC_{50}^D \sim 100$ μM, the concentration required to promote ATP occlusion with **TMR-Se** appeared to be lower ($EC_{50}^D = 14 \pm 7$ μM, Table 1, and Figure S1 of the Supporting Information). The 9-[4-(dimethylamino)phenyl]selenoxanthylium derivative **2** displayed a relatively higher value of K_m^D (288 ± 115 μM) with modest ATPase stimulation [1.65 ± 0.24 nmol min^{-1} μg^{-1} (Table 1)]. Derivative **2** also promoted ATP occlusion by A/A Pgp effectively ($EC_{50}^D = 43 \pm 37$ μM, Table 1, and Figure S1). Next, derivatives **3** and **4**, which displayed relatively weak ATPase stimulation with values of K_m^D that could not be accurately ascertained (or not measurable due to concentrations of available stock solutions), were tested for their ability to promote ATP occlusion by A/A Pgp. 9-(4-*N*-Morpholinophenyl)selenoxanthylium derivative **3** and 9-(1-naphthyl)selenoxanthylium derivative **4** were also effective in promoting ATP occlusion with EC_{50}^D values of 20 ± 11 and 0.4 ± 0.2 μM, respectively (Table 1 and Figure S1). The ability of the pentacyclic xanthylium derivatives **5** and **6** to elicit ATP occlusion in A/A was also examined. Derivatives **5** and **6** were also effective at promoting ATP occlusion by A/A Pgp with EC_{50}^D values of 9 ± 4 and 7 ± 6 μM, respectively (Table 1, Figure 2, and Figure S1).

For all of the derivatives, apparent EC_{50}^D values for promoting ATP occlusion were determined by fitting the data to the partition equation used previously to determine K_m^D values (*19, 48*). This formula incorporates a basal value that disappears as the drug site(s) becomes occupied. In this case, the basal value was the amount of ATP occlusion that occurs in a manner independent of drug and is ~0.4–0.5 mol/mol. Apparent EC_{50}^D values for stimulation of ATP occlusion are based upon earlier studies in which we demonstrated that drugs can dramatically affect the rate of ATP occlusion (*46*). Although the eventual stoichiometry of ATP occlusion always approaches one molecule of ATP per Pgp, the $t_{1/2}$ values for reaching saturation were ~1 and ~30 min in the presence and absence of drug, respectively (*44, 45*). It may be notable that in most cases, the concentration of **TMR** analogue required to facilitate ATP occlusion (EC_{50}^D values) appeared to be lower than the concentration required to confer ATPase stimulation. While these differences may be due to the assays employed or the type of Pgp utilized (wild-type vs A/A mutant), the data suggest that ATP occlusion is a more sensitive indicator of coupling.

*Competition of Analogues of **TMR** with VER As Assessed by ATPase Activity.* An ability to promote ATP occlusion effectively indicates that these derivatives occupy a drug pocket that communicates the transition to the engaged NBD dimer (ONC). Since this conformation is likely to be a critical intermediate in the catalytic pathway (*44, 45, 47*) and other drugs such as VER promote this conformation, we wanted to determine if binding by these analogues is competitive with VER. First, we tested the ability of the **TMR** analogues to inhibit VER-dependent ATPase activity. Since the analogues fail to elicit robust ATPase activity whereas VER elicits an approximate 10-fold rate enhancement above the basal level, we expected that this differential would permit reliable measurements and that the contributions from the **TMR** analogues to the observed ATPase activity might be effectively ignored. The effect of increasing concentrations of the **TMR** derivative on Pgp ATPase activity in the presence of a fixed, saturating concentration of VER (200 μM) was examined. These experiments revealed significant inhibition of VER-dependent ATPase activity, and all IC_{50} values were in the low micromolar range (Table 1). Additionally, except for the 1-naphthyl derivative **4**, which

displayed a very high propensity for ATP occlusion (EC_{50}^{D} $\sim$ 0.4 μM) and less ability to inhibit VER-stimulated ATPase activity (IC_{50} $\sim$ 30 μM, Table 1, and Figure S2), all IC_{50} values for inhibition of VER-dependent ATPase activity correlated reasonably well with EC_{50}^{D} values for ATP occlusion (Table 1). Figure 3a shows the inhibition pattern for the pentacyclic derivative **5**, and others are available in Figure S2 of the Supporting Information. This derivative was particularly notable since a best fit of the data suggests that the inhibition pattern may occur in two phases, with $\sim$10 μM being the cutoff between the two phases. Midpoint values for the phases were $\sim$0.3 and $\sim$40 μM, respectively (Figure 3a).

Importantly, we found that there was no lag in reactivation of Pgp ATPase activity after full inhibition by any of the **TMR** analogues. In this experiment, Pgp was preincubated with the **TMR** analogue at a concentration that displayed full inhibition. Next the samples were passed through centrifuge columns to remove unbound material, and VER-dependent ATPase activity was measured. In all cases, full activity was recovered (data not shown). This indicates reversibility of the interaction upon dilution (*65*) and demonstrates that the apparent decrease in activity is not due to permanent inactivation of Pgp by denaturation or by photoinactivation as previously described (*54*).

Since IC_{50} values merely demonstrate that Pgp activity can be slowed in the presence of these analogues but do not reveal if the **TMR** analogue is binding competitively with VER, we performed classical competitive analysis to address this question. All of the **TMR** analogues displayed apparent competitive inhibition patterns with VER. Figure 3b shows the apparent competitive inhibition pattern for compound **5**, and others are available in Figure S3 of the Supporting Information. All K_i values for the apparent competitive inhibition of VER-dependent ATPase by the **TMR** analogues are provided in Table 1. Competitive analysis is a well-established approach in general enzymology and has also been used to establish relationships between drugs in Pgp (*20*). In the case of Pgp, competitive effects of drugs on ATPase activity were reinforced by the fact that V_i displayed clear noncompetitive inhibition versus VER in this type of assay (*20*). Moreover, given that all of the **TMR** analogues that were examined displayed apparent competitive inhibition versus VER, it is likely that their binding sites at least partially overlap. However, we cannot entirely exclude the possibility that the inhibitory **TMR** analogues bind at multiple sites or that cooperative interactions between **TMR**s and VER may negatively affect turnover.

*Effect of **TMR** Analogues on ADP·V_i Trapping and Release.* Since this group of **TMR** analogues appears to be effective at promoting ATP occlusion yet confers relatively weak ATPase activity compared to VER, it is formally possible that a later step in the catalytic cycle may be slow or blocked. To address this possibility, we next assayed their ability to promote ADP·V_i trapping as well as the kinetics of ADP·V_i release. Evidence that the ADP·V_i trapped species closely mimics the ATP hydrolysis transition state comes from an X-ray crystal structure of myosin with ADP·V_i retained within its catalytic site (*66*) as well as biochemical studies with Pgp itself (*67, 68*). Effective ADP·V_i trapping may reveal a capacity to stabilize the transition state of hydrolysis per se (one step beyond ATP occlusion). To explore these possibilities, each analogue of **TMR** (final concentration of 200 μM) was included in standard ADP·V_i trapping reactions and passed through centrifuge columns to measure the amount of nucleotide retained after a 10 min incubation at 37 °C. All of the analogues effectively trapped ADP with V_i (Figure 4), and in no case were they able to promote tight nucleotide binding in the absence of V_i (data not shown). These data indicate that the **TMR** analogues elicit the interactions required to stabilize the transition state and that release of P_i appears to be normal. Next, we assessed the release of the ADP·V_i trapped complex in the presence of compounds **3** and **5** and compared the rates to those from experiments performed in parallel containing either VER or DMSO (no drug). In all cases, the rate of release of the ADP·V_i trapped complex was nearly identical with a $t_{1/2}$ of $\sim$40 min (Figure 5). These data suggest that the relatively slower turnover seen in the presence of this set of **TMR** analogues is not due to an alteration of the rate of ADP release.

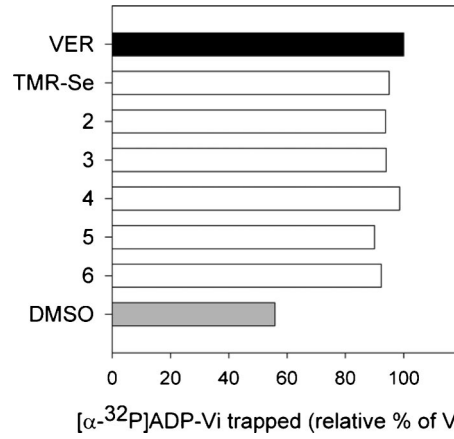

FIGURE 4: Effect of **TMR** analogues on ADP·V_i trapping. The effect of TMR analogues on ADP·V_i trapping was determined as described in Experimental Procedures. Data are the average of four experiments performed in duplicate using two different preparations of Pgp, and values showed excellent agreement (a standard deviation of less than 10% in all cases). One hundred percent trapping for VER represents $\sim$1 mol of ADP·V_i/mol of Pgp.

***TMR** Analogues Are Transported by Pgp.* Efflux of rhodamines has been used to define substrates and/or antagonists of Pgp (*49, 50*). Among the rhodamines and closely related analogues, **TMR** has been described as the best transport substrate for Pgp in viable MDR cells and using Pgp reconstituted in proteoliposomes (*69–71*). We examined the transport of 5 μM solutions of **TMR**, **TMR-S**, **1-S** (Chart 1), **5**, and **6** in monolayers of MDCK-MDR1 transfected cells, which overexpress Pgp (or ABCB1) (*72*). To evaluate the role of Pgp in the transport of the compounds of this series, we assessed transport in the absorptive (apical) and secretory (basolateral) transport direction of the cell monolayer and then calculated an efflux ratio ($P_{BA/AB}$) (*73*). We determined that addition of BSA to the buffer was required because a marked fraction of mass added to the donor equilibrated with the cell monolayer for some of the compounds, and this resulted in gross underestimation of the permeability constant (*74*). The assay was repeated in the presence of 2.5 μM LSN335984 (IC_{50} = 0.4 μM), which is structurally related to the Pgp-specific inhibitor LY335979 or zosquidar (*7*). The ratio $P_{BA/AB}$ can be normalized by dividing by the secretory/basal ratio observed in the fully

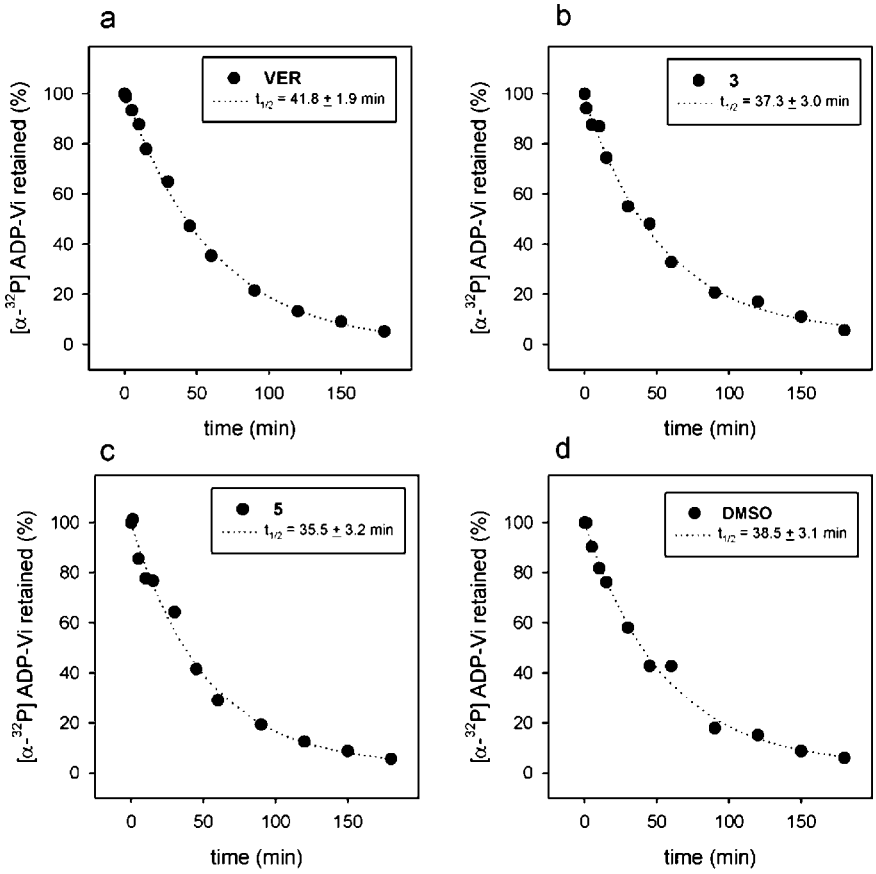

FIGURE 5: Effect of compounds **3** and **5** on the kinetics of ADP·V_i release. The effect of compounds **3** and **5** on the release of the ADP·V_i trapped complex was determined as described in Experimental Procedures. Data represent the mean of two separate experiments. Data sets showed excellent agreement with less than 5% error at each point. Dotted lines are the nonlinear least-squares regression fits of the data to single-exponential parameters, and in all cases, $R \sim 0.99$. Calculated $t_{1/2}$values are shown in the insets.

Table 2: Studies of **TMR** Analogues with MDCK-MDR1 Cells[a]

Compd	P_{AB} ($\times 10^{-6}$ cm s^{-1})	P_{BA} ($\times 10^{-6}$ cm s^{-1})	$P_{BA/AB}$	normalized ratio, $P_{BA/AB}$ (without inhibitor/with inhibitor)[b]	$P_{passive}$[c] ($\times 10^{-6}$ cm s^{-1})	% cell associated[d]	ratio (without inhibitor/with inhibitor)
TMR	0.30 ± 0.01	101 ± 1	338	217	1.7 ± 0.5	14.5 ± 0.9	4.3
TMR with inhibitor	1.4 ± 0.1	2.1 ± 0.2	1.6			63 ± 2	
TMR-S	0.60 ± 0.01	90 ± 12	149	114	3.4 ± 0.7	14 ± 1	5.1
TMR-S with inhibitor	3.0 ± 0.1	3.9 ± 0.2	1.3			71 ± 2	
1-S	0.67 ± 0.03	48 ± 4.5	71	45	1.6 ± 0.5	2.1 ± 0.2	3.8
1-S with inhibitor	1.2 ± 0.01	1.9 ± 0.2	1.6			8.0 ± 0.1	
5	1.6 ± 1.0	25 ± 4	15	17	1.23 ± 0.08	32.00 ± 0.03	2.0
5 with inhibitor	1.30 ± 0.08	1.2 ± 0.1	0.9			64 ± 3	
6	0.08 ± 0.01	36 ± 5	450	132	0.7 ± 0.6	30 ± 2	2.1
6 with inhibitor	0.33 ± 0.01	1.1 ± 0.3	3.4			64 ± 3	

[a] Values of transport in the absorptive (P_{AB}) and secretory (P_{BA}) mode in the absence or presence of inhibitor, the ratio of secretory to absorptive transport ($P_{BA/AB}$) in the absence or presence of inhibitor, the normalized ratio [$P_{BA/AB}$(no inhibitor)/$P_{BA/AB}$(with inhibitor)], the percent cell-associated **TMR** analogue in the absence or presence of inhibitor, and the ratio of cell-associated **TMR** analogue in the presence or absence of inhibitor. Details of the methods are provided in Experimental Procedures. Error limits represent the standard deviation. [b] The normalized ratio represents the $P_{BA/AB}$ ratio in the absence of inhibitor divided by the $P_{BA/AB}$ ratio in the presence of inhibitor. [c] $P_{passive}$ represents the mean of P_{AB} and P_{BA} in the fully inhibited system. [d] Percent cell associated is the fraction of mass extracted from the cell monolayer by a methanol wash after flux for 1 h in the AB direction.

inhibited system. Large efflux ratios are assumed to be due to high Pgp-mediated efflux of the compound. Values of transport in the absorptive (P_{AB}) and secretory (P_{BA}) mode in the absence or presence of inhibitor, the ratio of secretory to absorptive transport ($P_{BA/AB}$) in the absence or presence of inhibitor, the normalized ratio [$P_{BA/AB}$(no inhibitor)/$P_{BA/AB}$(with inhibitor)], the percent cell-associated **TMR** analogue in the absence or presence of inhibitor, and the ratio of cell-associated **TMR** analogue in the presence or absence of inhibitor are compiled in Table 2. (Additional examples of **TMR** analogues from ref *48* are shown in Figures S4 and S5 of the Supporting Information.)

As observed in earlier work (*69–71*), **TMR** was actively transported by Pgp in the MDCK-MDR1 cells with a normalized ratio ($P_{BA/AB}$) of 217. The other **TMR** analogues gave normalized ratios ($P_{BA/AB}$) that were smaller (114 for **TMR-S**, 45 for **1-S**, 17 for **5**, and 132 for **6**) but still quite large, suggesting active efflux by Pgp. The percent of cell-associated **TMR** analogue increased in each case in the presence of inhibitor. For **TMR**, the ratio of cell-associated

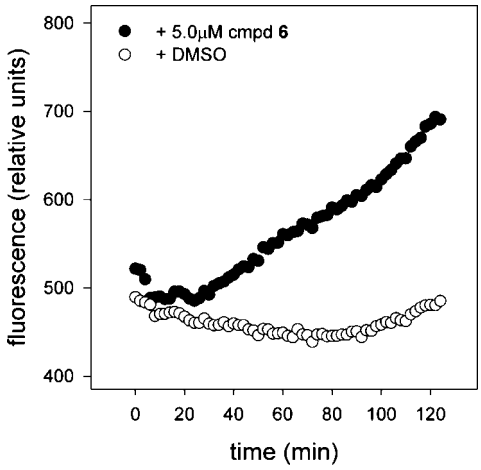

FIGURE 6: Kinetics of uptake of calcein-AM by CR1R12 cells. Persistent exclusion and enhanced uptake in the presence of compound **6**. Typical kinetic experiment demonstrating the robust enhancement of uptake of calcein-AM by TMR analogues. The calcein-AM assay is described in Experimental Procedures.

dye was 4.3 in the presence relative to absence of inhibitor. For **TMR-S** and **1-S**, this ratio was quite similar (5.1 and 3.8, respectively). For both **5** and **6**, the percent of cell-associated dye in the absence of inhibitor (30 ± 2 and 32 ± 0.3, respectively) was significantly larger ($p < 0.01$) than for **TMR**, **TMR-S**, or **1-S**. Furthermore, the increase in the percent of cell-associated dye in the presence of inhibitor for **5** and **6** was smaller with values of 2.0 and 2.1, respectively.

***TMR** Analogues Facilitate Uptake of Calcein-AM into CR1R12 and MDCK-MDR1 Cells.* CR1R12 cells are highly drug resistant Chinese hamster ovary cells that were derived from CH^{r}C5 cells for the purpose of generating high levels of plasma membrane Pgp for purification (*26*). CR1R12 cells have been used to demonstrate transport of both **TMR-S** and **TMR-Se** (*59*). The biochemistry described above suggests that **TMR-S**, **TMR-Se**, and **TMR** derivatives **2–6** bind to Pgp at a drug transport site and that these compounds are actively transported by Pgp. To test the idea that the **TMR** analogues affect drug transport in cells, we employed a calcein-AM (CAM) uptake assay. Extracellular CAM does not fluoresce; however, upon cellular uptake, cleavage of the four acetoxy methyl esters by intracellular esterases yields highly fluorescent calcein. CAM uptake (and exclusion) has been used extensively to probe Pgp activity in cells and is an accepted strategy for rapidly assessing Pgp inhibition (*75, 76*). We found that all of the analogues facilitated uptake of CAM in CR1R12 cells, and Figure 6 shows a typical kinetic uptake experiment comparing compound **6** to a control containing 2% DMSO without **6** added. In the absence of **6**, essentially zero CAM was converted to calcein, indicating that Pgp expression in the CR1R12 cells resulted in complete exclusion of CAM.

Values of EC_{50}^{CAM} for CAM uptake in CR1R12 cells in the presence of the **TMR** analogues were determined for **TMR-S** and derivatives **3–6**. The pentacyclic derivatives **5** and **6** were the most potent of these compounds, with data for these two compounds shown in Figure 7. (The slight decrease in fluorescence at higher concentrations shown in Figure 7 reflects increased absorption of calcein fluorescence by the dye chromophore at higher concentrations of **5** and **6**.) Uptake of CAM was followed kinetically, and relative fluorescence values obtained after a 2 h incubation at 37 °C were plotted as a function of the concentration of **TMR** derivative. In all experiments, the rates of CAM uptake were linear over the 20 min to 2 h interval, and any time point within this interval reflects the overall rate of CAM uptake. The apparent half-maximal concentration of the **TMR** analogue required to facilitate saturation of CAM uptake (EC_{50}^{CAM}) was determined by fitting the data at the 2 h time point (where calcein fluorescence was maximal in each assay) by nonlinear least-squares regression to a single-exponential increase. Compound **5** exhibited an EC_{50}^{CAM} of 0.8 ± 0.3 μM, and compound **6** exhibited an EC_{50}^{CAM} of 1.0 ± 0.5 μM; in both cases, the maximal relative fluorescence units (rfu) for saturation of apparent uptake were very similar. Both 9-(4-morpholinophenyl)selenoxanthylium (**3**) and 9-(1-napthyl)selenoxanthylium (**4**) derivatives displayed an EC_{50}^{CAM} of ~10 μM (Figure S6 of the Supporting Information), and interestingly, **TMR-S** displayed only modest enhancement even at 65 μM (data not shown).

Compounds **5** and **6** also facilitated the uptake of CAM into MDCK-MDR1 cells. Again, uptake of CAM was followed, and relative fluorescence values obtained after a 20 min incubation with CAM at 37 °C were plotted as a function of the concentration of the **TMR** derivative. In MDCK-MDR1 cells, compound **5** displayed an EC_{50}^{CAM} of 4.9 ± 0.6 μM and compound **6** displayed an EC_{50}^{CAM} of 4.7 ± 2.0 μM. In both cases, the maximal rfu for saturation of apparent uptake were very similar (~1300 rfu) and were similar to the relative fluorescence values for CAM uptake in the fully inhibited system (in the presence of 2.5 μM LSN335984, it gave an EC_{50}^{CAM} of 0.22 μM, and ~1400 rfu).

These data demonstrate that the **TMR** analogues facilitate CAM uptake and that a hierarchy in their effectiveness exists even among this small set. Taken in context with the biochemical data presented previously, CAM uptake will be an effective cellular assay for analyzing future derivatives of **TMR**.

DISCUSSION

The goal of this study was to build upon structure–activity relationships (SARs) for the recognition of **TMR** analogues by Pgp and to use the SARs to probe catalytic mechanism. The basic **TMR** scaffold was modified, and the new analogues were used to probe Pgp's drug binding pocket(s). The intention was to probe specifically the ability of **TMR** analogues to promote ATP occlusion compared to ATP hydrolysis. The most interesting finding was that many of the novel **TMR** analogues presented herein appear to be capable of eliciting ATP occlusion at concentrations where stimulation of ATP hydrolysis appears to be nearly compensatory to basal levels. Compared to other **TMR** analogues that confer robust ATP hydrolysis (even exceeding VER in some cases), they appear to be quite ineffective, yet their ability to promote ATP occlusion appears to be similar to that of the **TMR** derivatives that confer robust turnover. In these cases, ATP occlusion likely reveals the true affinity of the **TMR** analogue for the ATP-coupled drug binding site. These results further support the idea that the apparent affinity of a drug does not correlate with turnover. Further, in cases

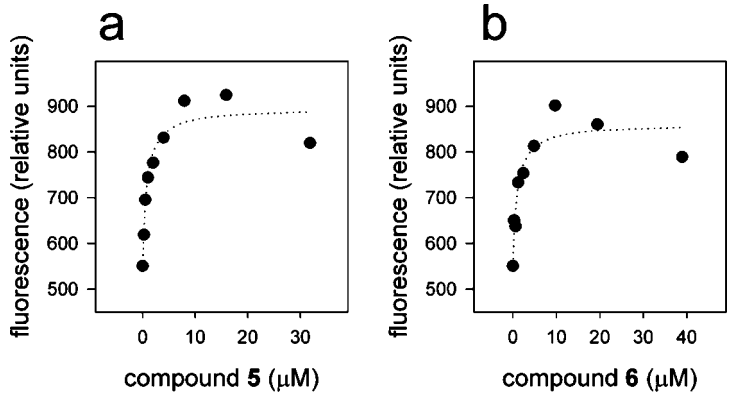

FIGURE 7: Enhancement of uptake of calcein-AM into CR1R12 cells by compounds **5** and **6**. Experiments were performed as described in the legend of Figure 6 (and see Experimental Procedures), except that the concentrations of compounds **5** and **6** were varied and the reading after 2 h is plotted. EC_{50}^{D} values for enhancement of calcein-AM uptake were 0.79 ± 0.43 and 0.95 ± 0.42 μM for compounds **5** and **6**, respectively (see also Table 1).

where ATPase appears exactly compensatory to basal values, an ability to promote ATP occlusion is a sensitive indicator of the transition to the coupled form.

Previously, we found a few **TMR** analogues which conferred turnover as high as VER (~4–5 nmol min^{-1} μg^{-1}) with relatively lower K_m^D values [~5 μM; see compounds **21** and **22** in ref *48* labeled as **1-S** and **1-Se**, respectively, in this study). This suggested that the **TMR** scaffold is intrinsically capable of eliciting robust turnover given the correct modification. What are the properties of the inhibitory **TMR** analogues that distinguish them from those that confer robust turnover? It is notable that a modification as subtle as tying the amine alkyl groups back to the xanthylium core through propano bridges or conversion of the phenyl moiety at the 9-position of **TMR** to a naphthalene group could dramatically impact turnover. Since a high-resolution X-ray structure of Pgp is unavailable, an exhaustive analysis is not reasonable. However, in the literature, many suggestions for molecular descriptors that confer inhibitory properties exist and may prove to be informative (*77*). First, in cases that are otherwise equivalent for H-bonding, overall size, surface area, and hydrophobicity may be contributing factors, especially since modeling predicts that the vestibule is largely hydrophobic (*78*). In addition, an increased potential for $\pi-\pi$ or cation$-\pi$ interactions may also contribute to a slower overall turnover rate (*78*). Relative to **TMR-S**, 9-(1-naphthyl)selenoxanthylium derivative **4** and pentacyclic derivative **5** have increased overall size and surface area, which will contribute to hydrophobicity (log *P*, the *n*-octanol/water partition coefficient, values of 1.80 and 2.4 for **4** and **5**, respectively, vs a log *P* value of −0.07 for **TMR-S**). Furthermore, the Se atoms in the core do not form strong H-bonds relative to O and S atoms, which further weakens H-bonding in **4** and **5**. Finally, the 9-(1-naphthyl) substituent of **4** can contribute to an increased number of $\pi-\pi$ interactions, while the julolidyl fragment of **5** and **6** is more electron rich from the two additional alkyl substituents, which will also contribute to an increased number of $\pi-\pi$ or cation$-\pi$ interactions.

Given the lack of competition for cross-linking sites by MTS derivatives of VER and rhodamine previously reported by the Clarke laboratory (*79*), is it legitimate to think of these **TMR** analogues as binding competitively with VER? In fact, in their pharmacophore model for rhodamines, Pajeva and Weise (*25*) suggest that VER and rhodamines display compatible features. Namely, the hydrophobic site H2 in the VER pharmacophore is positioned between two H-bond acceptor sites, A1 and A2. The same arrangement is found in the **TMR** analogues with a benzo-fused ring (H2) of the xanthylium core situated between the chalcogen atom of the core (A1) and the amino substituent at the 3- or 6-position (A2). The VER pharmacophore has a second hydrophobic aromatic group, H1, that is essentially orthogonal (88° dihedral) to the first, while the 9-aryl substituents of the **TMR** derivatives (H1) are held orthogonal to the xanthylium core. With regard to the MTS−VER cross-linking data presented by the Clarke laboratory, constitutive activation of turnover after drug cross-linking at a high-affinity site would be somewhat surprising if the system is tightly coupled and drug release from OFF sites is required for turnover. Thus, constitutive activation after cross-linking may reflect a certain degree of permissiveness to vestibule occupancy and suggests that drug release may not be required for turnover or that multiple drug binding sites exist within the "vestibule". Considering these possibilities, the **TMR** analogues presented herein will be useful reagents for testing competitive drug site occupancy.

The Pgp transport studies with MDCK-MDR1 cells indicated that both **TMR** and **TMR-S**, which confer modest ATP hydrolysis, compound **1-S** with a high rate of turnover for ATP hydrolysis, and compounds **5** and **6** with minimal turnover for ATP hydrolysis (Table 2) are all substrates for Pgp. These data indicate that all of the compounds bind to transport sites even if they confer ATPase activities that manifest at near-basal levels. EC_{50}^{CAM} values (CAM uptake) in the CR1R12 cells and EC_{50}^{D} (ATP occlusion in the A/A mutant) are similar for these compounds with values of ~100 μM for **TMR-S** and values on the order of 1 μM for **5** and **6**. Collectively, these data suggest that compounds **5** and **6** modulate Pgp to allow more of themselves or other drugs to enter the cell relative to **TMR-S**. It is important to recognize in these data that the primary structural difference between **TMR**, **TMR-S**, and **TMR-Se** and **5** and **6** is the two propano bridges linking one of the dimethylamino substituents in **TMR**, **TMR-S**, and **TMR-Se** back to the rosamine core in **5** and **6**. This subtle difference has striking implications for the response of Pgp both as the isolated protein and in Pgp-expressing cells. The effectiveness of the **TMR** analogues

in cells also reinforces the idea that these compounds display a relatively high affinity for Pgp in a native membrane environment. This is critical since lipid composition and fluidity may greatly influence interaction of drugs with Pgp (*7, 9, 18*). The combined biochemical and cellular data suggest that these **TMR** derivatives are tightly bound in a substrate (drug) binding pocket.

The study of cooperative effects (both positive and negative) by multiple drugs within a common pocket is a current topic of interest among ABC transport proteins, including Pgp (*80–82*). The case of ABCC1 or MRP-1 is particularly intriguing since it appears that reduced glutathione (GSH) may stimulate transport of other drugs by facilitating the conformational transition that engages the catalytic sites, and presumably the carrier reorientation event (*83*). The results presented herein may prove to be informative in terms of understanding rate-determining parameters for transport since the drug site chemistry that allows Pgp to properly engage its catalytic sites has not been forthcoming. Our long-term goal is to build a pharmacophore model for drug binding that disentangles parameters that lead to affinity as well as turnover.

ACKNOWLEDGMENT

We gratefully acknowledge Alan Senior, Robert Bambara, and Barbara Iglewski for encouragement. We also gratefully acknowledge Matt Disney and Barbara Iglewski for the use of their space for radioactive experiments. Finally, we thank the reviewers whose efforts and suggestions greatly improved the manuscript. Views and opinions of and endorsements by the author(s) do not reflect those of the U.S. Army or the U.S. Department of Defense.

SUPPORTING INFORMATION AVAILABLE

Promotion of ATP occlusion by **TMR-Se** and compounds **2–4** and **6** (Figure S1), inhibition of VER-dependent ATPase by compounds **2–4** and **6** (Figure S2), competitive inhibition of VER-dependent ATPase activity by compounds **2–4** and **6** (Figure S3), and enhancement of uptake of calcein-AM into CR1R12 cells by compounds **3** and **4** (Figure S4). This material is available free of charge via the Internet at http://pubs.acs.org.

REFERENCES

1. Gottesman, M. M., and Ling, V. (2006) The molecular basis of multidrug resistance in cancer: The early years of P-glycoprotein research. *FEBS Lett. 580*, 998–1009.
2. Ambudkar, S. V., Kim, I., and Sauna, Z. (2006) The power of the pump: Mechanisms of action of P-glycoprotein (ABCB1). *Eur. J. Pharm. Sci. 27*, 392–400.
3. Al-Shawi, M. K., and Omote, H. (2005) The remarkable transport mechanism of P-glycoprotein: A multidrug transporter. *J. Bioenerg. Biomembr. 37*, 489–496.
4. Callaghan, R., Ford, R. C., and Kerr, I. D. (2006) The translocation mechanism of P-glycoprotein. *FEBS Lett. 580*, 1056–1063.
5. Higgins, C. F., and Linton, K. J. (2004) The ATP switch model for ABC transporters. *Nat. Struct. Mol. Biol. 11* (10), 918–926.
6. Loo, T. W., and Clarke, D. M. (2005) Do drug substrates enter the common drug-binding pocket of P-glycoprotein through "gates"? *Biochem. Biophys. Res. Commun. 329*, 419–422.
7. Seelig, A., and Gatlik-Landwojtowicz, E. (2005) Inhibitors of multidrug efflux transporters: Their membrane and protein interactions. *Mini-Rev. Med. Chem. 5* (2), 135–151.
8. Raub, T. J. (2006) P-Glycoprotein recognition of substrates and circumvention through rational drug design. *Mol. Pharmaceutics 3*, 3–25.
9. Stein, W. D. (1998) Kinetics of the P-glycoprotein, the multidrug transporter. *Exp. Physiol. 83*, 221–232.
10. Szakacs, G., Paterson, J. K., Ludwig, J. A., Booth-Genthe, C., and Gottesman, M. M. (2006) Targeting multidrug resistance in cancer. *Nat. Rev. Drug Discovery 5*, 219–234.
11. Litman, T., Druley, T. E., Stein, W. D., and Bates, S. E. (2001) From MDR to MXR: New understanding of multidrug resistance systems, their properties and clinical significance. *Cell. Mol. Life Sci. 58*, 931–959.
12. Leonard, G. D., Fojo, T., and Bates, S. E. (2003) The role of ABC transporters in clinical practice. *Oncologist 8*, 411–424.
13. Dean, M. (2005) The genetics of ATP-binding cassette transporters. *Methods Enzymol. 400*, 409–429.
14. Chloupkova, M., Pickert, A., Lee, J. Y., Souza, S., Trinh, Y. T., Connelly, S. M., Dumont, M. E., Dean, M., and Urbatsch, I. L. (2007) Expression of 25 human ABC transporters in the yeast *Pichia pastoris* and characterization of the purified ABCC3 ATPase activity. *Biochemistry 46*, 7992–8003.
15. Senior, A. E., al-Shawi, M. K., and Urbatsch, I. L. (1995) The catalytic cycle of P-glycoprotein. *FEBS Lett. 377* (3), 285–289.
16. Sauna, Z. E., and Ambudkar, S. V. (2000) Evidence for a requirement for ATP hydrolysis at two distinct steps during a single turnover of the catalytic cycle of human P-glycoprotein. *Proc. Natl. Acad. Sci. U.S.A. 97*, 2515–2520.
17. van Veen, H. W., Margolles, A., Muller, M., Higgins, C. F., and Konings, W. N. (2000) The homodimeric ATP-binding cassette transporter LmrA mediates multidrug transport by an alternating two-site (two-cylinder engine) mechanism. *EMBO J. 19*, 2503–2514.
18. Omote, H., and Al-Shawi, M. K. (2006) Interaction of transported drugs with the lipid bilayer and P-glycoprotein through a solvation exchange mechanism. *Biophys. J. 90*, 4046–4059.
19. Al-Shawi, M. K., Polar, M. K., Omote, H., and Figler, R. A. (2003) Transition state analysis of the coupling of drug transport to ATP hydrolysis by P-glycoprotein. *J. Biol. Chem. 278* (52), 52629–52640.
20. Litman, T., Zeuthen, T., Skovsgaard, T., and Stein, W. D. (1997) Competitive, non-competitive and cooperative interactions between substrates of P-glycoprotein as measured by its ATPase activity. *Biochim. Biophys. Acta 1361* (2), 169–176.
21. Martin, C., Berridge, G., Higgins, C. F., Mistry, P., Charlton, P., and Callaghan, R. (2000) Communication between multiple drug binding sites on P-glycoprotein. *Mol. Pharm. 58* (3), 624–632.
22. Dey, S., Ramachandra, M., Pastan, I., Gottesman, M. M., and Ambudkar, S. V. (1997) Evidence for two nonidentical drug-interaction sites in the human P-glycoprotein. *Proc. Natl. Acad. Sci. U.S.A. 94* (20), 10594–10599.
23. Maki, N., Hafkemeyer, P., and Dey, S. (2003) Allosteric modulation of human P-glycoprotein. Inhibition of transport by preventing substrate translocation and dissociation. *J. Biol. Chem. 278* (20), 18132–18139.
24. Crivori, P., Reinach, B., Pezzetta, D., and Poggesi, I. (2006) Computational models for identifying potential P-glycoprotein substrates and inhibitors. *Mol. Pharmaceutics 3*, 33–44.
25. Pajeva, I. K., and Wiese, M. (2002) Pharmacophore model of drugs involved in P-glycoprotein multidrug resistance: Explanation of structural variety (hypothesis). *J. Med. Chem. 45* (26), 5671–5686.
26. Al-Shawi, M. K., and Senior, A. E. (1993) Characterization of the adenosine triphosphatase activity of Chinese hamster P-glycoprotein. *J. Biol. Chem. 268* (6), 4197–4206.
27. Sarkadi, B., Price, E. M., Boucher, R. C., Germann, U. A., and Scarborough, G. A. (1992) Expression of the human multidrug resistance cDNA in insect cells generates a high activity drug-stimulated membrane ATPase. *J. Biol. Chem. 267*, 4854–4858.
28. Omote, H., and Al-Shawi, M. K. (2002) A novel electron paramagnetic resonance approach to determine the mechanism of drug transport by P-glycoprotein. *J. Biol. Chem. 277* (47), 45688–45694.
29. Higgins, C. F., and Gottesman, M. M. (1992) Is the multidrug transporter a flippase? *Trends Biochem. Sci. 17*, 18–21.
30. Seelig, A., and Landwojtowicz, E. (2000) Structure-activity relationship of P-glycoprotein substrates and modifiers. *Eur. J. Pharm. Sci. 12* (1), 31–40.
31. Lee, J. Y., Urbatsch, I. L., Senior, A. E., and Wilkens, S. (2002) Projection structure of P-glycoprotein by electron microscopy.

Evidence for a closed conformation of the nucleotide binding domains. *J. Biol. Chem. 277* (42), 40125–40131.
32. Lee, J. Y., Urbatsch, I. L., Senior, A. E., and Wilkens, S. (2007) Nucleotide-induced structural changes in P-glycoprotein observed by electron microscopy. *J. Biol. Chem.* (in press).
33. Rosenberg, M. F., Velarde, G., Ford, R. C., Martin, C., Berridge, G., Kerr, I. D., Callaghan, R., Schmidlin, A., Wooding, C., Linton, K. J., and Higgins, C. F. (2001) Repacking of the transmembrane domains of P-glycoprotein during the transport ATPase cycle. *EMBO J. 20* (20), 5615–5625.
34. Rosenberg, M. F., Callaghan, R., Modok, S., Higgins, C. F., and Ford, R. C. (2005) Three-dimensional structure of P-glycoprotein: The transmembrane regions adopt an asymmetric configuration in the nucleotide-bound state. *J. Biol. Chem. 280* (4), 2857–2862.
35. Loo, T. W., and Clarke, D. M. (2002) Vanadate trapping of nucleotide at the ATP-binding sites of human multidrug resistance P-glycoprotein exposes different residues to the drug-binding site. *Proc. Natl. Acad. Sci. U.S.A. 99* (6), 3511–3516.
36. Loo, T. W., Bartlett, M. C., and Clarke, D. M. (2003) Drug binding in human P-glycoprotein causes conformational changes in both nucleotide-binding domains. *J. Biol. Chem. 278* (3), 1575–1578.
37. Sonveaux, N., Shapiro, A. B., Goormaghtigh, E., Ling, V., and Ruysschaert, J. M. (1996) Secondary and tertiary structure changes of reconstituted P-glycoprotein. A Fourier transform attenuated total reflection infrared spectroscopy analysis. *J. Biol. Chem. 271*, 24617–24624.
38. Mechetner, E. B., Schott, B., Morse, B. S., Stein, W. D., Druley, T., Davis, K. A., Tsuruo, T., and Roninson, I. B. (1997) P-Glycoprotein function involves conformational transitions detectable by differential immunoreactivity. *Proc. Natl. Acad. Sci. U.S.A. 94*, 12908–12913.
39. Druley, T. E., Stein, W. D., and Roninson, I. B. (2001) Analysis of MDR1 P-glycoprotein conformational changes in permeabilized cells using differential immunoreactivity. *Biochemistry 40*, 4312–4322.
40. Sonveaux, N., Vigano, C., Shapiro, A. B., Ling, V., and Ruysschaert, J. M. (1999) Ligand-mediated tertiary structure changes of reconstituted P-glycoprotein. A tryptophan fluorescence quenching analysis. *J. Biol. Chem. 274* (25), 17649–17654.
41. Liu, R., Siemiarczuk, A., and Sharom, F. J. (2000) Intrinsic fluorescence of the P-glycoprotein multidrug transporter: Sensitivity of tryptophan residues to binding of drugs and nucleotides. *Biochemistry 39*, 14927–14938.
42. Qu, Q., and Sharom, F. J. (2001) FRET analysis indicates that the two ATPase active sites of the P-glycoprotein multidrug transporter are closely associated. *Biochemistry 40*, 1413–1422.
43. Loo, T. W., and Clarke, D. M. (2005) Recent progress in understanding the mechanism of P-glycoprotein-mediated drug efflux. *J. Membr. Biol. 206*, 173–185.
44. Tombline, G., Bartholomew, L. A., Urbatsch, I. L., and Senior, A. E. (2004) Combined mutation of catalytic glutamate residues in the two nucleotide binding domains of P-glycoprotein generates a conformation that binds ATP and ADP tightly. *J. Biol. Chem. 279*, 31212–31220.
45. Tombline, G., Muharemagic, A., White, L. B., and Senior, A. E. (2005) Involvement of the "occluded nucleotide conformation" of P-glycoprotein in the catalytic pathway. *Biochemistry 44*, 12879–12886.
46. Tombline, G., and Senior, A. E. (2005) The occluded nucleotide conformation of p-glycoprotein. *J. Bioenerg. Biomembr. 37*, 497–500.
47. Sauna, Z. E., Kim, I., Nandigama, K., Kopp, S., Chiba, P., and Ambudkar, S. V. (2007) Catalytic Cycle of P-glycoprotein: Evidence for Formation of the ES Reaction Intermediate with ATPγS, a Nonhydrolyzable Analogue of ATP. *Biochemistry 46*, 13787–13799.
48. Tombline, G., Donnelly, D. J., Holt, J. J., You, Y., Ye, M., Gannon, M. K., Nygren, C. L., and Detty, M. R. (2006) Stimulation of P-Glycoprotein ATPase by Analogues of Tetramethylrosamine: Coupling of Drug Binding at the "R" Site to the ATP Hydrolysis Transition State. *Biochemistry 45*, 8034–8047.
49. Lee, J. S., Paull, K., Alvarez, M., Hose, C., Monks, A., Grever, M., Fojo, A. T., and Bates, S. E. (1994) Rhodamine efflux patterns predict P-glycoprotein substrates in the National Cancer Institute drug screen. *Mol. Pharm. 46*, 627–638.
50. Scala, S., Akhmed, N., Rao, U. S., Paull, K., Lan, L.-B., Dickstein, B., Lee, J.-S., Elgemeie, G. H., Stein, W. D., and Bates, S. E. (1997) P-Glycoprotein Substrates and Antagonists Cluster into Two Distinct Groups. *Mol. Pharm. 51*, 1024–1033.
51. Detty, M. R., Prasad, P. N., Donnelly, D. J., Ohulchanskyy, T., Gibson, S. L., and Hilf, R. (2004) Synthesis, properties, and photodynamic properties in vitro of heavy-chalcogen analogues of tetramethylrosamine. *Bioorg. Med. Chem. 12*, 2537–2544.
52. Wagner, S. J., Skripchenko, A., Donnelly, D. J., Ramaswamy, K., and Detty, M. R. (2005) Chalcogenoxanthylium photosensitizers for the photodynamic purging of blood-borne viral and bacterial pathogens. *Bioorg. Med. Chem. 13*, 5927–5935.
53. Del Valle, D. J., Donnelly, D. J., Holt, J. J., and Detty, M. R. (2005) 2,7-Bis-N,N-dimethylaminochalcogeno-xanthen-9-ones via Electrophilic Cyclization with Phosphorus Oxychloride. *Organometallics 24*, 3807–3810.
54. Holt, J. J., Gannon, M. K., II, Tombline, G., McCarty, T. A., Page, P. M., Bright, F. V., and Detty, M. R. (2006) A cationic chalcogenoxanthylium photosensitizer effective in vitro in chemosensitive and multidrug-resistant cells. *Bioorg. Med. Chem. 14*, 8635–8643.
55. Lerner-Marmarosh, N., Gimi, K., Urbatsch, I. L., Gros, P., and Senior, A. E. (1999) Large scale purification of detergent-soluble P-glycoprotein from *Pichia pastoris* cells and characterization of nucleotide binding properties of wild-type, Walker A, and Walker B mutant proteins. *J. Biol. Chem. 274* (49), 34711–34718.
56. Tombline, G., Urbatsch, I. L., Virk, N., Muharemagic, A., White, L. B., and Senior, A. E. (2006) Expression, purification, and characterization of cysteine-free mouse P-glycoprotein. *Arch. Biochem. Biophys. 445*, 124–128.
57. Segel, I. H. (1975) *Enyme Kinetics*, John Wiley & Sons, New York.
58. Tombline, G., Bartholomew, L. A., Tyndall, G. A., Gimi, K., Urbatsch, I. L., and Senior, A. E. (2004) Properties of P-glycoprotein with mutations in the "catalytic carboxylate" glutamate residues. *J. Biol. Chem. 279*, 46518–46526.
59. Gibson, S. L., Hilf, R., Donnelly, D. J., and Detty, M. R. (2004) Analogues of tetramethylrosamine as transport molecules for and inhibitors of P-glycoprotein-mediated multidrug resistance. *Bioorg. Med. Chem. 12*, 4625–4631.
60. Hopfner, K. P., Karcher, A., Shin, D. S., Craig, L., Arthur, L. M., Carney, J. P., and Tainer, J. A. (2000) Structural biology of Rad50 ATPase: ATP-driven conformational control in DNA double-strand break repair and the ABC-ATPase superfamily. *Cell 101*, 789–800.
61. Smith, P. C., Karpowich, N., Millen, L., Moody, J. E., Rosen, J., Thomas, P. J., and Hunt, J. F. (2002) ATP binding to the motor domain from an ABC transporter drives formation of a nucleotide sandwich dimer. *Mol. Cell 10* (1), 139–149.
62. Locher, K. P., Lee, A. T., and Rees, D. C. (2002) The *E. coli* BtuCD structure: A framework for ABC transporter architecture and mechanism. *Science 296* (5570), 1091–1098.
63. Chen, J., Lu, G., Lin, J., Davidson, A. L., and Quiocho, F. A. (2003) A tweezers-like motion of the ATP-binding cassette dimer in an ABC transport cycle. *Mol. Cell 12* (3), 651–661.
64. Oloo, E. O., and Tieleman, D. P. (2004) Conformational transitions induced by the binding of MgATP to the vitamin B12 ATP-binding cassette (ABC) transporter BtuCD. *J. Biol. Chem. 279* (43), 45013–45019.
65. Deves, R., and Krupka, R. M. (1989) Inhibition kinetics of carrier systems. *Methods Enzymol. 171*, 113–132.
66. Smith, C. A., and Rayment, I. (1996) X-ray structure of the magnesium(II) ·ADP·vanadate complex of the *Dictyostelium discoideum* myosin motor domain to 1.9 Å resolution. *Biochemistry 35* (17), 5404–5417.
67. Urbatsch, I. L., Sankaran, B., Weber, J., and Senior, A. E. (1995) P-Glycoprotein is stably inhibited by vanadate-induced trapping of nucleotide at a single catalytic site. *J. Biol. Chem. 270*, 19383–19390.
68. Urbatsch, I. L., Tyndall, G. A., Tombline, G., and Senior, A. E. (2003) P-Glycoprotein catalytic mechanism: Studies of the ADP-vanadate inhibited state. *J. Biol. Chem. 278* (25), 23171–23179.
69. Eytan, G. D., Regev, R., Hurwitz, C. D., and Assaraf, Y. G. (1997) Efficiency of P-glycoprotein-mediated exclusion of rhodamine dyes from multidrug-resistant cells is determined by their passive transmembrane movement rate. *Eur. J. Biochem. 248*, 104–112.
70. Lu, P., Liu, R., and Sharom, F. J. (2001) Drug transport by reconstituted P-glycoprotein in proteoliposomes: Effect of substrates and modulators, and dependence on bilayer phase state. *Eur. J. Biochem. 268*, 1687–1695.
71. Loetchutinat, C., Saengkhae, C., Marbeuf-Gueye, C., and Garnier-Suillerot, A. (2003) New insights into the P-glycoprotein-mediated effluxes of rhodamines. *Eur. J. Biochem. 270*, 476–485.

72. Evers, R., Kool, M., Smith, A. J., van Deemter, L., de Haas, M., and Borst, P. (2000) Inhibitory effect of the reversal agents V-104, GF120918 and Pluronic L61 on MDR1Pgp-, MRP1- and MRP2-mediated transport. *Br. J. Cancer 83*, 366–374.
73. Troutman, M. D., and Thakker, D. R. (2003) Rhodamine 123 requires carrier-mediated influx for its activity as a P-glycoprotein substrate in Caco-2 Cells. *Pharm. Res. 20*, 1192–1199.
74. Sawada, G. A., Barsuhn, C. L., Lutzke, B. S., Houghton, M. E., Padbury, G. E., Ho, N. F. H., and Raub, T. J. (1999) Increased lipophilicity and subsequent cell partitioning decrease passive transcellular diffusion of novel, highly-lipophilic antioxidants. *J. Pharm. Exp. Ther. 288*, 1317–1326.
75. Essodaigui, M., Broxterman, H. J., and Garnier-Suillerot, A. (1998) Kinetic analysis of calcein and calcein-acetoxymethylester efflux mediated by the multidrug resistance protein and P-glycoprotein. *Biochemistry 37*, 2243–2250.
76. Garnier-Suillerot, A., Marbeuf-Gueye, C., Salerno, M., Loetchutinat, C., Fokt, I., Krawczyk, M., Kowalczyk, T., and Priebe, W. (2001) Analysis of drug transport kinetics in multidrug-resistant cells: Implications for drug action. *Curr. Med. Chem. 8*, 51–64.
77. Klopman, G., Shi, L. M., and Ramu, A. (1997) Quantitative structure-activity relationship of multidrug resistance reversal agents. *Mol. Pharmacol. 52*, 323–334.
78. Pawagi, A. B., Wang, J., Silverman, M., Reithmeier, R. A., and Deber, C. M. (1994) Transmembrane aromatic amino acid distribution in P-glycoprotein. A functional role in broad substrate specificity. *J. Mol. Biol. 235*, 554–564.
79. Loo, T. W., Bartlett, M. C., and Clarke, D. M. (2003) Methanethiosulfonate derivatives of rhodamine and verapamil activate human P-glycoprotein at different sites. *J. Biol. Chem. 278* (50), 50136–50141.
80. Acharya, P., Tran, T. T., Polli, J. W., Ayrton, A., Ellens, H., and Bentz, J. (2006) P-Glycoprotein (P-gp) Expressed in a Confluent Monolayer of hMDR1-MDCKII Cells Has More Than One Efflux Pathway with Cooperative Binding Sites. *Biochemistry 45*, 15505–15519.
81. Borst, P., Zelcer, N., van de Wetering, K., and Poolman, B. (2006) On the putative co-transport of drugs by multidrug resistance proteins. *FEBS Lett. 580*, 1085–1093.
82. Deeley, R. G., and Cole, S. P. (2006) Substrate recognition and transport by multidrug resistance protein 1 (ABCC1). *FEBS Lett. 580*, 1103–1111.
83. Manciu, L., Chang, X. B., Buyse, F., Hou, Y. X., Gustot, A., Riordan, J. R., and Ruysschaert, J. M. (2003) Intermediate structural states involved in MRP1-mediated drug transport. Role of glutathione. *J. Biol. Chem. 278*, 3347–3356.

BI7021393